Proceedings of the 2016 IEEE
International Conference on Robotics and Biomimetics
Qingdao, China, December 3-7, 2016

Design, Fabrication and Kinematic Modeling of a 3D-motion Soft Robotic Arm

Zheyuan Gong, Zhexin Xie, Xingbang Yang, Tianmiao Wang and Li Wen*, *Member, IEEE*

Abstract— **In this paper, we present the design, fabrication and the mathematical model of an entire soft robotic arm with three-dimensional (3D) locomotion. We first describe the design of the soft arm based on 3D printed channels that were spatially distributed at the interface of two different silicone elastomeric materials which enable complex 3D motion of the soft arm. Then we demonstrate the workspace of motion at different air pressure levels, and the ability of the mathematic model to predict the three-dimensional movement in free space. We further demonstrate that modifying the texture of the surface of the soft arm can constrain the radial expansion. Finally, we estimate the workspace, location repeatability of the soft arm via actual tests.**

I. Introduction

Soft robotics is a new member of the robotic family that has several promising features, such as lightweight, inexpensive, easily fabricated, simply to control, etc. [1]. The soft robotics can be fabricated by several approaches including multi-material 3D printing [2], shape deposition manufacturing (SDM) [3], soft lithography [4], or integrated multiple manufacturing approaches to create composite materials[5]-[7]. Variable-length tension cables [8],[9], pneumatic or hydraulic for pressurization of channels in a soft material [10], and dielectric elastomer [11], electro-active polymers or shape memory alloy [12]-[14] are usually used for the actuation of soft robotics. While integrating multiple segments of soft actuators has made several bio-inspired robotic locomotions possible [16],[17].

With soft deformable bodies, animals in nature tend to find a simple but efficient way to interact with the environments. Many cephalopods such as octopus [16] have exceptional manipulation and locomotion abilities even without rigid skeletons. Their bodies are mainly composed of intrinsically soft materials that can deform by the muscles and absorb the considerable energy of the collision during locomotion. Soft pneumatic robots can distribute pressure uniformly over large areas without elaborate controls; this capability makes it possible for them to manipulate fragile and irregular objects [18]-[22].

The mobility of the soft robotic gripper with which we have worked out structures actuated by the expansion of elastomeric pneumatic networks – have been limited to a single bending mode in the direction defined by the anisotropy of the pneumatic expansion [24]. In this paper, we wish to improve the motion capabilities of these systems, and specifically to fabricate and mathematically model entire soft robotic arm with three-dimensional (3D) motion. This paper describes the design and fabrication of the soft robotic arm based on 3D printed channels spatially distributed at the interface of two different silicone elastomeric materials; these composite elastomeric structures enable complex 3D motion of the soft arm. We demonstrate that modifying the texture of the surface of the soft arm can constrain the radial expansion. Based on the kinematic model, we further demonstrate both workspace of motion at different air pressure levels, and the ability of the mathematic model to predict the three-dimensional movement in free space.

II. Materials and Methods

A. Design and Fabrication

The soft robotic arm is designed to achieve three-dimensional motion by pneumatic actuation. Individual chambers are used to actuate the soft arm to bend in multiple directions and motions. We applied the modularized design and fabrication. Each module of the segment has three individual chambers which allow the module bending in 3 DOFs. And more identical modules are integrated to obtain more DOFs. In this section, we demonstrated a 2-module-segment soft robotic arm. We used a silicone elastomer (Dragon Skin 10, Smooth-on, USA) and a polydimethylsiloxane (PDMS) to fabricate soft robotic arm. Dragon Skin 10 has a Shore A hardness of 10, used to fabricate the outer layer, including the three individual chambers. PDMS has a Shore A hardness of 50, which limits deformation in contrast to Dragon Skin 10. As a result, because of the elongation difference between the outer layer and the central core, when actuated by compressed air the module can perform independently omnidirectional bending. Specially, the surface of soft arm is designed as corrugate texture, and we cover the rubber tendons in the groove of corrugate. Therefore, the texture and tendons constrain radial ballooning of the chambers and thus the expansion mainly contributed to length increment. Compared with previous works [18],[20], we can see that our soft arm could achieve bending motions in less radial ballooning (as shown in figures of next sections).

The fabrication of this three-dimensional soft robotic arm is a process of multiple-step casting procedures. We fabricated the soft arm in silicone elastomer with the three-dimensional printed molds made of Polylactic Acid (PLA) plastic. Fig. 1 demonstrates the process we used to fabricate the soft arm. The main idea is to cast each single segment individually in steps (a)-(d), and then in step (e) we connect these modules from below upward to form the soft

Research supported by the National Science Foundation support projects, China, under contract number 61403012, National Science Foundation support key projects, China, under contract number 61333016, and Beijing Science Foundation support projects under contract number 4154077.

The authors are with the School of Mechanical Engineering and Automation, Beihang University, Beijing, 100191, People's Republic of China; *corresponding author e-mail for contact: liwen@buaa.edu.cn.

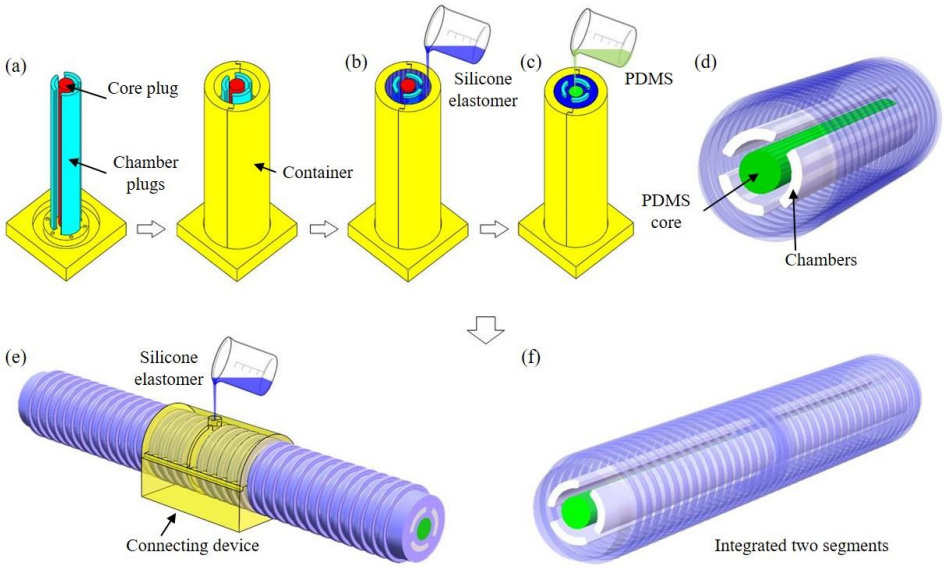

Figure 1. Fabrication of a soft robotic arm. (a) 3D printed mold for a single segment soft arm, where the chamber plugs and core plug are used to form the core and chambers; (b) fill the mold with Dragonskin 10; (c) remove the center template and cast with PDMS; (d) single segment removed from the mold; (e) integrate two segments with connecting device filled with Dragonskin 10; (f) the integrated double segments of soft robotic arm.

robotic arm. In step (f), the two segments soft arm were unmolded, and then we filled 8mm-length sections at both ends of the soft arm with silicone elastomer to seal the six chambers. Six silicone tubes were inlet into the soft arm, which could be used to deliver compressed air to activate the soft arm. The total time required for fabrication was approximately ten hours. Before this process, we used computer aided design (CAD) to design the molds. A 3D printer (Makerbot Replicator 5, MakerBot, USA) manufactured the molds with PLA from the CAD files. To reduce the adhesion between PLA molds and elastomer, the release agent was used to treat the surface of PLA molds to make the soft arm and PLA molds separate easily. To fabricate multiple segments manipulator, step (e) will be repeated for several times. Meanwhile, we constrain the radial ballooning of each segment with rubber tendons.

B. Kinematics modeling

The soft robotic arm shown in this paper is composed of two soft segments, while each segment contains a 2-DOF bending section and two indeformable death-sections due to the specific fabrication process (elongation is also another DOF, but it's quite small that we ignore this DOF), as shown in Fig. 2(a). Under the interaction of six chambers within two segments, the soft robotic arm has 4 DOFs. The six independent chambers can be actuated with comprised air, where the position and orientation can be controlled by programmed pressure.

Fig. 2(b) shows the overview of modeling process of the soft robotic arm. The modeling process could be divided into two parts: (1) the relationship between pressure (p_{ij}, the subscripts i and j mean segment i chamber j, the same as follows) and length of chambers (l_{ij}); (2) the transformation from chamber length (l_{ij}) to the coordinate of the end of soft arm (x_i, y_i, z_i). Because of the nonlinear response of soft material such as silicon elastomer, it's complex to figure out (1) theoretically, so we finish this task via experiments. In this section, we mainly illustrate the transformation from length to coordinate. Obviously, the pneumatic driven soft robotic arm is a continuum robot. Considering the previous works on PCC (Piecewise Constant Curvature [23]), we make assumptions as follow:

a) The curvature rate is constant in a bending section, while the indeformable section presents a line;
b) The chambers of a segment are parallel, and the cross sections are equal in the same section;
c) To reduce the complexity of modeling, the soft arm is analyzed without gravity and load.

The reason for choosing length as the parameter to describe the actuated condition is: although the length, swelling volume, curvature and wall thickness of chambers are all the monotonic reflections of different actuated conditions in different pressure, we choose length mainly taking into consideration the simplification for measurement. As known, swelling volume and wall thickness are complicated in measuring except using special equipment. Moreover, it's not easy to describe the bending directions in 3D space with curvature.

1) *Robot-independent transformation:* Based on the assumptions, we could simplify the soft robotic arm as independently controlled constant curves and lines, shown in Fig. 1(b). Q_0 is the base static coordinate system, while Q_{ib} and Q_{il} represent the end of bending section and death section in the ith segment. These transformations could be easily described by homogeneous matrixes:

$$T = \begin{bmatrix} R & p \\ 0 & 1 \end{bmatrix} \tag{1}$$

Where R is the rotation matrix and p is the translation vector. Considering all the segments are actuated in the same way, it could be clear to figure out the transformation in a single segment, shown in Fig. 2(c). Actually, this bending translation could be regarded as the rotation about y-axis with

curvature angle θ_i the rotation about z-axis with orientation angle φ_i. We define that the x-axis pointing to the center of circle and z-axis coinciding with the tangent of the circle. Thus, we need to post-multiply the homogeneous matrix with the rotation matrix R(-φ_i) and zero translation. The final form of the transformation matrix for one bending section is shown as follows:

$$ {}^{(i-1)1}_{ib}T = \begin{bmatrix} c^2\phi_i c\theta_i + s^2\phi_i & c\phi_i s\phi_i(c\theta_i - 1) & c\phi_i s\theta_i & rc\phi_i(1-c\theta_i) \\ c\phi_i s\phi_i(c\theta_i - 1) & s^2\phi_i c\theta_i + c^2\phi_i & s\phi_i s\theta_i & rs\phi_i(1-c\theta_i) \\ -c\phi_i s\theta_i & -s\phi_i s\theta_i & c\theta_i & rs\theta_i \\ 0 & 0 & 0 & 1 \end{bmatrix} \quad (2) $$

Where $c\theta_i$=cosθ_i, and $s\theta_i$=sinθ_i, the same to φ_i.

Meanwhile, the transformation matrix of non-deformable section could be written as follows obviously:

$$ {}^{ib}_{il}T = \begin{bmatrix} 1 & 0 & 0 & 0 \\ 0 & 1 & 0 & 0 \\ 0 & 0 & 1 & d_{si} \\ 0 & 0 & 0 & 1 \end{bmatrix} \quad (3) $$

Where d_{si} is the length of the death section of the ith segment.

Thus, the homogeneous matrix for whole segment transformation could be written as equation (4). And the different segments used in the calculation were shown in Fig. 2(d). From the combination of different segments and sections and the homogeneous matrix for a single segment, we can deduce the global transformation matrix as equation (5).

$$ {}^{(i-1)1}_{il}T = {}^{(i-1)1}_{ib}T \cdot {}^{ib}_{il}T \quad (4) $$

$$ {}^{0}_{nl}T = {}^{0}_{11}T \cdot {}^{11}_{2l}T \cdots {}^{(n-1)1}_{nl}T \quad (5) $$

Particularly, the soft robotic arm we used has two segments and 6 DOFs. So when n=2, we could work out the specific transformation for our soft arm as follows:

$$ {}^{0}_{2l}T = {}^{0}_{11}T \cdot {}^{11}_{2l}T \quad (6) $$

When we want to know the exact coordinate of the tip on the soft arm in the base static coordinate system, post-multiply a vector [0;0;0;1] which describes the tip's location in Q_{2l}.

2) Robot-specific transformation: The destination of our transformation is to represent the location parameter (x_i, y_i, z_i) with chambers length (l_{ij}). In the previous statement, we have already combined the location parameter (x_i, y_i, z_i) and (κ_i, φ_i, θ_i) which is regarded as the intermediate parameters. The relation between the chamber length (l_{ij}) and the intermediate parameters (κ_i, φ_i, θ_i) is presented as follows.

The assumptions on the same cross section and parallel chamber allow question simplified so that we could analyze random cross sections regardless of the expansion of chambers. According to the geometric diagram shown in Fig. 2(e), it is easy to calculate the expression of intermediate parameters (κ_i, φ_i, θ_i). Where l_{i1} means the length of chamber 1 in the ith segment, and d means the distance between cross section center and the center in the outer wall of the chamber. Particularly, we use the outer wall center mainly considering the accessible for measurement. By the way, we also exclude the influence of expansion of the chamber in measurement, which will be described in detail in experiments.

$$ \kappa_i = \frac{1}{r_i} = \frac{2\sqrt{l_{i1}^2 + l_{i2}^2 + l_{i3}^2 - l_{i1}l_{i2} - l_{i1}l_{i3} - l_{i2}l_{i3}}}{(l_{i1} + l_{i2} + l_{i3})d} \quad (7) $$

$$ \phi_i = \tan^{-1}\left(\frac{l_{i2} + l_{i3} - 2l_{i1}}{\sqrt{3}(l_{i2} - l_{i3})}\right) \quad (8) $$

$$ \theta_i = \frac{2\sqrt{l_{i1}^2 + l_{i2}^2 + l_{i3}^2 - l_{i1}l_{i2} - l_{i1}l_{i3} - l_{i2}l_{i3}}}{3d} \quad (9) $$

Thus, we combine the chambers length (l_{ij}) and location parameter (x_i, y_i, z_i) together.

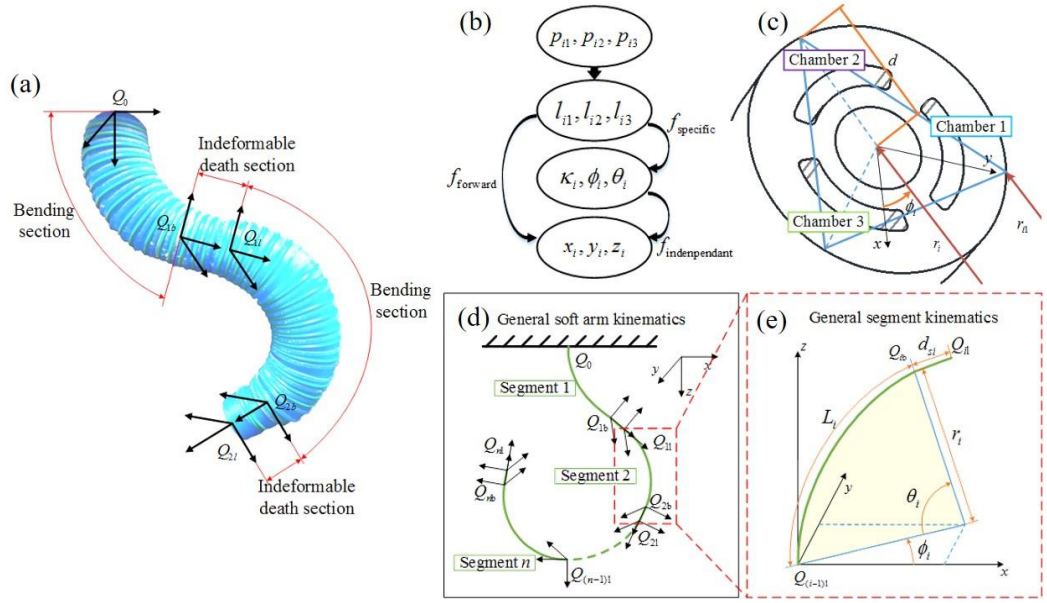

Figure 2. Kinematics modeling: (a) the global view of modeling. The main idea of this transform is to represent the ith segment position parameters (x_i, y_i, z_i) using length parameters (l_i) via arc parameters (κ_i, φ_i, θ_i), and figure out the relation between actuation parameter (p_i) and length (l_i). Thus, we could predict position when we set pressure; (b) the cross section of soft arm which shows the 3 actuating chambers and its geometrical relationship; (c) general kinematics model for soft arm; (d) general kinematics model for a segment. The bending section could be considered as a perfect arc of circle whose length is L_i, while indeformable section as a line whose length is d_{si}.

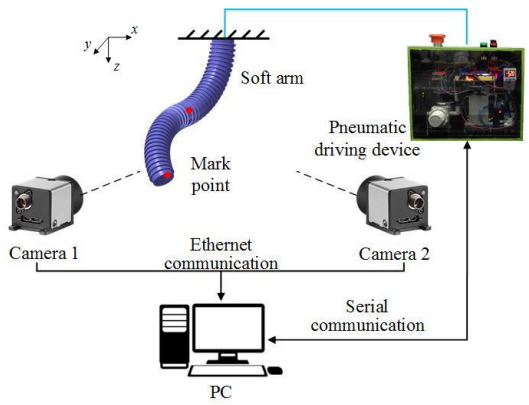

Figure 4. Overview of the soft arm experiments set up. The soft arm is driven by a pneumatic device controlled by PC. Meanwhile its 3D motions are rebuilt via 2 cameras, which makes coordinates of the mark points accessible.

C. Experiments setup

To explore the relation between the pressure and length of the pneumatic chamber, and validate the kinematic modeling based controlling, we have set up an experimental platform based on binocular vision. Fig. 3 shows the experiments set up. The soft robotic arm was driven by a pneumatic driving device which was established by us and could set pressure of all six chambers via proportional valves (ITV0030-2BL, SMC, Japan). Meanwhile, mark points on the soft arm in different actuated condition could be recorded by two stereo cameras (acA1600-60gc, BASLER, German). Thus, the variable motions of the soft arm could be rebuilt by a motion analysis software ProAnalyst (ProAnalyst, Xcitex, USA), which makes the coordinates of mark points accessible. The soft robotic arm and stereo cameras were fixed on a 600mm×500mm×400mm frame. Two cameras were located 48mm apart while the angle between cameras and soft arm was approximately 63°. Also, the images were conveyed through PCI-E Ethernet interface and the pneumatic driving device communicated with PC by the serial port.

Before experiments, we carefully calibrated the workspace of stereo cameras. Making use of the calibration board (PA-3DP-24, Xcitex, USA) appended to ProAnalyst, we figured out the error in stereo space of camera, which is shown in TABLE. I. The data in TABLE. I is given by ProAnalyst.

1) *Pressure-length identification:* Although the previous statement combines the chambers length (l_{ij}) and location parameter (x_i, y_i, z_i) together, we directly use pressure (p_i) as the actuation parameters. And we can figure out the curve on pressure and chambers length. Because of the nonlinear response in soft material expanding, bending and elongating, it's not easy to solve the relation between chambers length and pressure in a theoretical way. Thus, we try to design an experiment to achieve this.

TABLE I. ERROR OF STEREO CAMERAS SPACE

Average error (mm)	Standard deviations (mm)	Maximum error (mm)	Minimum error (mm)
0.6381	**0.2484**	**1.1573**	**0.2891**

To measure the different length of different chambers actuated in various pressures, we analyzed the 1600pixels×1200pixels images of different segments in soft arm actuated by the pneumatic driving device in different pressures. We actuated the segment 1 (upper segment, which is shown in Fig. 2(c)) and segment 2 (lower segment) separately in diverse pressures (40 kPa, 50 kPa, 60 kPa, 70 kPa, and 80 kPa). In each group, we repeated for five times and measured the length of the bending sections in 3 chambers. In addition, all the measurements were done in calibrated images. To avoid the influence of expanding on the pressurized chamber, we chose the curve for bending section (yellow line in Figs. 5(a) and (b)) that parallel to center curve (red dotted line in Figs. 5(a) and (b)) as the chamber length.

2) *Kinematic model based location error:* We performed this experiment to compare the real mark points location obtained by stereo cameras and model-based predicted position and analyze the location error of the kinematic model. In order to evaluate the three-dimensional positioning capability under the kinematic model, the binocular vision was used to rebuild motion and measure the coordinate of mark points. The measured position was given by the 3D motion analysis software ProAnalyst, while the predicted location was given by the MATLAB (MATLAB R2015b, Mathworks, USA) simulation. In the binocular vision measurement, we actuated chambers to make the soft robotic arm in "S" motion. In MATLAB simulation, we used the measured chambers length as the input to calculate the position of tips. We made the comparison in pressures 40 kPa, 50 kPa, 60 kPa, 70 kPa, and 80 kPa, while five times repetition for each pressure.

III. RESULTS

A. Workspace simulation

Fig. 4 shows the kinematic model based simulation on the workspace of one segment and a double segments soft robotic arm. The workspace of single segment clearly shows three-dimensional motion accessible to the soft robotic arm. The morphology of single-segment workspace shapes part of sphere face (covers approximately 10mm×10mm×8mm volume) with thickness caused by the elongation of chambers. Meanwhile, using interaction on multiple chambers, the soft robotic arm performs 6 DOFs in different motions and shows a hollow sphere workspace. The size of the accessible zone is approximately 40mm-diameter sphere while the hollow

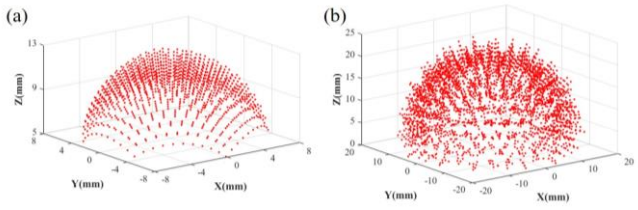

Figure 3. Simulations on workspace of soft arm based on kinematics model: (a) simulation for the single segment which shows workspace shaped sphere face with thickness; (b) double segments workspace simulation which is a hollow sphere. The base of soft arm is set at (0,0,0).

diameter is about 28mm. In general, two-segment soft arm collects more accessible space.

B. *Length – pressure identification*

We performed the experiment to figure out the relation between chambers length and pressure for different segments. The results show that the pressure has a great impact on the chamber length. Meanwhile, the response to pressure changing on two segments is quite different. From Fig. 5, it can be observed that the chambers elongate with the pressure increase in the both segments. Under 80 kPa, the chamber in segment one was measured as 117.2 mm and 53.95% for elongation. In contrast length for segment two was measured as 174.0 mm and 95.51% for elongation. This rise occurs slowly when pressure is relatively low (10~50kPa), while the length increases much more rapidly after 50 kPa. In the comparison between segment 1 and 2, we can see that the upper segment bent less than the other one in high pressure (more than 70 kPa), and this deviation has an upward trend.

C. *Kinematic model based location error*

Fig. 6 demonstrates the location error in different pressures. It is quite obvious that in relatively low pressure (no more than 70 kPa), the experimental curve fits theoretical prediction well, where the location errors stay in a low level that is less than 5.8 mm. In addition, the error bars are quite short when pressure is no more than 70 kPa. The maximum standard deviation appears when pressure is 60 kPa, under which the exact value is 0.59 mm. The small level of standard deviation shows that the soft robotic arm performs well repeatability in low pressure. Moreover, we could see that the location error increases when the pressure rises. Before 70 kPa, the increment remains stable, while the location error rises steeply in 80 kPa and the value is 39.5 mm. Meanwhile, the standard deviation also rises to 3.32 mm, which represents a larger repeatable error. Overall, kinematic based control shows good performance when pressure is no more than 70 kPa. More interactive details of the soft arm motion can be found in the supplementary videos.

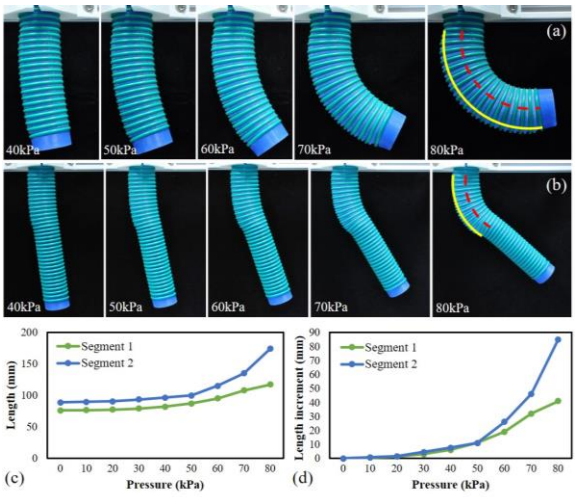

Figure 5. Identification for pressure and length. (a) and (b) show segment 1 and segment 2 bending when actuated separately in different pressures. Segment 1 shown in (b) bends less than segment 2 shown in (a); (c) shows the curvature about length measured and pressure, while (d) shows the per unit length increments of segments change when pressure rises. In the same pressure, the length of segment 2 increases more than that of segment 1. Red dotted line in (a) and (b) represents the center curve of a chamber, and yellow line is chamber length we measured.

IV. Discussion and Conclusion

Although there were some previous studies on three-dimensional soft bodied elastomers, few of them have quantitatively analyzed an open-loop kinematic model, which could help us achieve better understanding on the bio-inspired controlling principle of soft robot. In this paper, we demonstrated a pneumatic actuated, highly compliance, modularized soft robotic arm. The novel design and fabrication to integrate a multiple-segment soft robotic arm and constrain the radial expansion was expounded. We focused on the kinematic modeling which transforms pressure (p_i) to location parameters (x_i, y_i, z_i). Therefore, we could predict the position of soft arm tip by the pressure interaction in chambers. We first quantitatively analyzed the capability of an open-loop kinematic model without vision or sensors feedback compared with previous works [18][21], which will help us achieve better understanding on how the chambers interact to achieve complex motions and precise location.

The simulation demonstrated in Fig. 4 shows the sphere shaped workspace of soft robotic arm, which provides a persuasive evidence that three-dimensional motion is accessible as we designed. The morphology of working space contains a sphere hollow inside, which is quite similar to conventional robotic arm. The empty part is mainly due to that the maximum curvature of bending segments is limited by material and structure, while that on traditional robotic arm is caused by interference of joints. Moreover, in contrast between Fig. 4(a) and (b), it is obvious that we could enhance the workspace and reduce hollow diameter by integrating more segments of soft arms, which is quite significant on the potential applications for soft arm manipulation.

The chamber length has a monotonic relation with pressure. The chamber length increment becomes more rapid at high pressure. This change in rate probably is influenced by the nonlinear material properties and air compressibility in balloon chambers. Meanwhile, segment 1 bended less than the other one in high pressure, which could be well explained that segment 2 could be considered as load on segment 1, and the more it bends, the larger moment of force will generate. The moment caused by load reduces the bending curvature, which should be paid more attention when integrating more segments or operating in loading condition.

In this paper, we first quantitatively analyzed the capability of an open-loop kinematic model, and tested the location error of open-loop model based control without vision or sensors feedback [18][21]. The results will help us achieve better understanding on how the chambers interact to achieve complex motions and precise location. The location error has been considered as an essential indication for the kinematics control. The model based location was proved to have a good performance (less than 2.8 mm error) under low pressure. While operating under high pressure, the location error increases significantly. We hypothesized that the large deformation might cause it under high pressure, we didn't

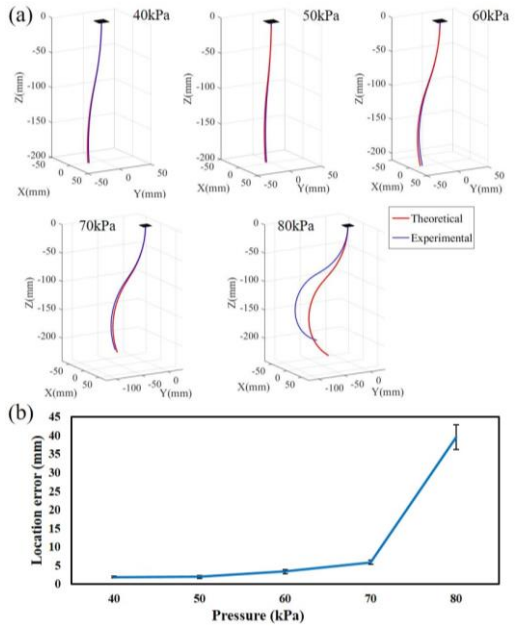

Figure 6. Location error influenced by pressure. The location error is defined as the Euclidean distance of theoretical point and average experimental data points. (a) The bending condition in contrast between theoretical point and experimental points, which shows the deviation of tips position. The red curve is given by theoretical simulation based on kinematic model and the blue one by experiment; (b) the location error changes with pressure, and stay in a low level when pressure is no more than 70kPa.

consider the effect of the balloon effect of the chambers that were inflated along the radial directions. Therefore, the geometric relations in the cross sections of the soft arm have been altered in a way that should further model via more detailed experiments (see Fig. 2(c) for notation). As both sides of the soft robotic segment have been filled with non-chambered soft materials which are non-extendable, the main expansion happens in the middle part of the chamber. This effect is remarkable under high pressure, nevertheless, could be ignored under low air pressure.

ACKNOWLEDGMENT

Many thanks to Yufei Hao for his assistance on design of this soft arm and contributions on this paper. This work was supported by the National Science Foundation support projects, China, under contract number 61403012, National Science Foundation supports key projects, China, under contract number 61333016, and Beijing Science Foundation support projects under contract number 4154077.

REFERENCES

[1] D. Rus and M. T. Tolley, "Design, fabrication and control of soft robots," Nature, vol. 521, pp. 467-75, 2015.

[2] N. W. Bartlett, M. T. Tolley, J. T. B. Overvelde, J. C. Weaver, B. Mosadegh, K. Bertoldi, et al., "A 3D-printed, functionally graded soft robot powered by combustion," Science, vol. 349, pp. 161-165, Jul 10 2015.

[3] S. A. Suresh, D. L. Christensen, E. W. Hawkes, and M. Cutkosky, "Surface and Shape Deposition Manufacturing for the Fabrication of a Curved Surface Gripper," Journal of Mechanisms and Robotics-Transactions of the Asme, vol. 7, May 2015.

[4] S. A. Morin, R. F. Shepherd, S. W. Kwok, A. A. Stokes, A. Nemiroski, and G. M. Whitesides, "Camouflage and Display for Soft Machines," Science, vol. 337, pp. 828-832, Aug 17 2012.

[5] K. J. Cho, J. S. Koh, S. Kim, W. S. Chu, Y. Hong, and S. H. Ahn, "Review of manufacturing processes for soft biomimetic robots," International Journal of Precision Engineering and Manufacturing, vol. 10, pp. 171-181, Jul 2009.

[6] A. A. Stokes, R. F. Shepherd, S. A. Morin, F. Ilievski, and G. M. Whitesides, "A Hybrid Combining Hard and Soft Robots," Soft Robotics, vol. 1, pp. 70-74, 2014.

[7] F. Connolly, P. Polygerinos, C. J. Walsh, and K. Bertoldi, "Mechanical Programming of Soft Actuators by Varying Fiber Angle," Soft Robotics, vol. 2, pp. 26-32, 2015.

[8] L. U. Odhner, L. P. Jentoft, M. R. Claffee, N. Corson, Y. Tenzer, R. R. Ma, et al., "A compliant, underactuated hand for robust manipulation," International Journal of Robotics Research, vol. 33, pp. 736-752, Apr 2014.

[9] C. H. Yeow, A. T. Baisch, S. G. Talbot, and C. J. Walsh, "Cable-Driven Finger Exercise Device With Extension Return Springs for Recreating Standard Therapy Exercises," Journal of Medical Devices-Transactions of the Asme, vol. 8, Mar 2014.

[10] B. Mosadegh, P. Polygerinos, C. Keplinger, S. Wennstedt, R. F. Shepherd, U. Gupta, et al., "Pneumatic Networks for Soft Robotics that Actuate Rapidly," Advanced Functional Materials, vol. 24, pp. 2163-2170, Apr 2014.

[11] A. Girard, J. P. L. Bigue, B. M. O'Brien, T. A. Gisby, I. A. Anderson, and J. S. Plante, "Soft Two-Degree-of-Freedom Dielectric Elastomer Position Sensor Exhibiting Linear Behavior," Ieee-Asme Transactions on Mechatronics, vol. 20, pp. 105-114, Feb 2015.

[12] Q. Shen, T. Wang, J. Liang, and L. Wen, "Hydrodynamic performance of a biomimetic robotic swimmer actuated by02ionic polymer–metal composite," Smart Materials & Structures, vol. 22, pp. 2896-2912, 2013.

[13] S. Seok, C. D. Onal, K. J. Cho, R. J. Wood, D. Rus, and S. Kim, "Meshworm: A Peristaltic Soft Robot with Antagonistic Nickel Titanium Coil Actuators," Ieee-Asme Transactions on Mechatronics, vol. 18, pp. 1485-1497, Oct 2013.

[14] J. S. Koh and K. J. Cho, "Omega-Shaped Inchworm-Inspired Crawling Robot With Large-Index-and-Pitch (LIP) SMA Spring Actuators," Ieee-Asme Transactions on Mechatronics, vol. 18, pp. 419-429, Apr 2013.

[15] K. Suzumori, S. Endo, T. Kanda, N. Kato, and H. Suzuki, "A Bending Pneumatic Rubber Actuator Realizing Soft-bodied Manta Swimming Robot," in Robotics and Automation, 2007 IEEE International Conference on, 2007, pp. 4975-4980.

[16] C. Laschi, M. Cianchetti, B. Mazzolai, L. Margheri, M. Follador, and P. Dario, "Soft Robot Arm Inspired by the Octopus," Advanced Robotics, vol. 26, pp. 709-727, 2012.

[17] C. D. Onal and D. Rus, "Autonomous undulatory serpentine locomotion utilizing body dynamics of a fluidic soft robot," Bioinspiration & Biomimetics, vol. 8, Jun 2013.

[18] A. D. Marchese and D. Rus, "Design, Kinematics, and control of a soft spatial fluidic elastomer manipulator." *Int. J. Robotics Research*, 2015.

[19] R. V. Martinez, C. R. Fish, X. Chen and G. M. Whitesides, "Elastomeric Origami: Programmable Paper-Elastomer Composites as Pneumatic Actuators." *Advanced Functional Materials*, 22.7:1376–1384, 2012.

[20] R. V. Martinez, J. L. Branch, C. R. Fish, L. Jin, R. F. Shepherd and R. M. D. Nunes, et al. "Robotic tentacles with three-dimensional mobility based on flexible elastomers. " Advanced Materials 25.2:205-12, 2013.

[21] X. Wang, T. Geng, Y. Elsayed, C. Saaj and C. Lekakou, "A unified system identification approach for a class of pneumatically-driven soft actuators." *Robotics & Autonomous Systems*, 63:136-149, 2015.

[22] C. Escande, T. Chettibi, R. Merzouki, V. Coelen and P. M. Pathak, "Kinematic Calibration of a Multi-section Bionic Manipulator." *IEEE/ASME Trans. Mechatronics*, pp. 663-674, Feb 20 2014.

[23] R. J. Webster, and B. A. Jones, "Design and Kinematic Modeling of Constant Curvature Continuum Robots: A Review." *International Journal of Robotics Research* 29.13:1661-1683, 2010.

[24] Y. Hao, Z. Gong, Z. Xie, S. Guan, X. Yang, Z. Ren, T. Wang and L. Wen, "Universal soft pneumatic robotic gripper with variable effective length." *Chinese Control Conf.*, to be published.